Theor Chem Acc (2012) 131:1273
DOI 10.1007/s00214-012-1273-0

REGULAR ARTICLE

Density functional theory for the description of charge-transfer processes at TTF/TCNQ interfaces

Tanguy Van Regemorter · Maxime Guillaume · Gjergji Sini · John S. Sears · Victor Geskin · Jean-Luc Brédas · David Beljonne · Jérôme Cornil

Received: 27 April 2012 / Accepted: 28 August 2012 / Published online: 15 September 2012

Abstract In the field of organic electronics, a central issue is to assess how the frontier electronic levels of two adjacent organic layers align with respect to one another at the interface. This alignment can be driven by the presence of a partial charge transfer and the formation of an interface dipole; it plays a key role for instance in determining the rates of exciton dissociation or exciton formation in organic solar cells or light-emitting diodes, respectively. Reliably modeling the processes taking place at these interfaces remains a challenge for the computational chemistry community. Here, we review our recent theoretical work on the influence of the choice of density functional theory (DFT) methodology on the description of the charge-transfer character in the ground state of TTF/TCNQ model complexes and interfaces. Starting with the electronic properties of the isolated TTF and TCNQ molecules and then considering the charge transfer and resulting interface dipole in TTF/TCNQ donor–acceptor stacks and bilayers, we examine the impact of the choice of DFT functional in describing the interfacial electronic structure. Finally, we employ computations based on periodic boundary conditions to highlight the impact of depolarization effects on the interfacial dipole moment.

Keywords DFT · Partial charge transfer · TTF/TCNQ · Organic electronics · Interface dipole · Interfaces

Published as part of the special collection of articles celebrating theoretical and computational chemistry in Belgium.

T. Van Regemorter (✉) · M. Guillaume · V. Geskin · D. Beljonne · J. Cornil
Laboratory for Chemistry of Novel Materials, University of Mons, Place du Parc 20, 7000 Mons, Belgium
e-mail: tanguy.vanregemorter@umons.ac.be

G. Sini · J. S. Sears · J.-L. Brédas
School of Chemistry and Biochemistry and Center for Organic Photonics and Electronics, Georgia Institute of Technology, 30332-0400 Atlanta, Georgia

G. Sini
Laboratoire de Physicochimie des Polymères et des Interfaces (LPPI), Université de Cergy-Pontoise, 5 Gay-Lussac, 95031 Cergy-Pontoise Cedex, France

1 Introduction

A key characteristic of organic electronic devices is their multilayered structure resulting in the presence of multiple interfaces that have a large impact on the overall device performance. Thus, a detailed understanding of the processes taking place between the layers is of crucial importance. The Schottky–Mott model is the simplest picture that can be applied to interfaces between organic conjugated materials. In this model, two adjacent layers share a common vacuum level at the interface. If this were to hold true, the energetic characteristics of the interface could be designed by tailoring separately the electronic properties of the two materials. However, numerous experimental studies based in particular on photoemission electron spectroscopy have demonstrated that this picture is usually not valid [1, 2]. In fact, an additional electrostatic potential is generally present at the donor/acceptor interface and shifts the vacuum level of one layer with respect to the other; this, in turn, modulates the relative alignment of the electronic levels of the interfacial components [3]. This additional potential is associated with the formation of an interface dipole layer (IDL); the IDL originates in charge-transfer processes between the donor and acceptor molecules and/or in polarization effects induced by the asymmetry of the electrostatic environment at the interface

as compared to the bulk of the individual materials [4, 5]. In the case of donor and acceptor moieties that are weakly coupled, either a vanishing or a complete charge transfer is expected. In the latter instance, a multiconfigurational quantum chemical approach is needed to properly account for the biradical character of the charge-transfer state [6]. In contrast, in cases where there is significant overlap between the molecular orbitals of the two components, a partial charge transfer is expected. In a one-electron picture, this implies that a fraction of an electron is transferred from the highest occupied levels of the donor to the lowest unoccupied levels of the acceptor. In the context of perturbation theory, the contribution of each possible charge-transfer pathway is proportional to the electronic coupling between the two relevant molecular orbitals and inversely proportional to their energy separation [7]. In small molecules that exhibit large energy differences between consecutive frontier electronic levels, the transfer is generally dominated by the coupling between the HOMO of the donor and LUMO of the acceptor (since this corresponds to the lowest energy pathway), except when symmetry effects make this coupling negligible.

In order to assess the most appropriate quantum mechanical methodology to describe a partial interfacial charge transfer and its contribution to the interface dipole, we have chosen to investigate a model interface consisting of a strong donor, the tetrathiafulvalene molecule (TTF), and a strong acceptor, the tetracyanoquinodimethane molecule (TCNQ). These molecules are known to present a significant charge transfer when in a parallel configuration [8].

In this contribution, we survey our recent theoretical work addressing the choice of the functional in density functional theory (DFT) to describe the charge-transfer character in the ground state of TTF/TCNQ model complexes [9, 10]. First, we examine how the nature of the functional impacts the electronic properties of isolated TTF or TCNQ molecules or stacks of each species. Through comparison to benchmark calculations, we then examine the impact of the functional choice on the computed charge transfer and associated interface dipole in TTF/TCNQ stacks. This study encompasses hybrid DFT functionals with a low percentage of HF exchange (B3LYP [11, 12], TPSSh [13], B97-1 [14–16], and PBE0 [16]), hybrid functionals with a high percentage of HF exchange (BMK [17], BHandH [18], BHLYP [18], M05-2X [19], M06-2X [20], and M06-HF [20]), and long-range corrected (LRC) functionals, also referred to as ω-functionals hereafter (ωB97X [21], ωB97X-D [22], as well as LRC-ωPBEh [23]). The influence of the basis set will not be discussed here since it was previously shown to play only a minor role in comparison with the choice of functional for the properties of interest [10]. Finally, we consider the influence of the environment on the interface dipole and partial charge transfer via depolarization effects.

2 Theoretical results

2.1 Isolated molecules

In this section, we investigate the impact of the percentage of exact exchange (% HF) on the computed electronic properties of isolated TTF and TCNQ molecules. In Fig. 1a, we present the evolution of the energy of the HOMO (highest occupied molecular orbital) and HOMO-1 level of an isolated TTF molecule and of the LUMO (lowest unoccupied molecular orbital) level of an isolated TCNQ molecule from several DFT functionals with varying amounts of HF exchange. Figure 1b shows the evolution of the corresponding donor/acceptor gap (E[$LUMO_{TCNQ}$]-E[$HOMO_{TTF}$]). It is worth noting that these values evolve linearly as a function of the percentage of HF exchange in the functional.

In the limit of large separation, the fundamental gap of a TTF/TCNQ complex should approach the difference between the ionization potential (IP) of TTF and the electron affinity (EA) of TCNQ. However, in the case of semilocal DFT functionals, the HOMO values differ largely from the IP and provide a HOMO–LUMO gap far below (by over 1 eV) the fundamental gap. This is due to the lack of derivative discontinuity (the finite jump in the exchange-correlation potential when passing through an integer

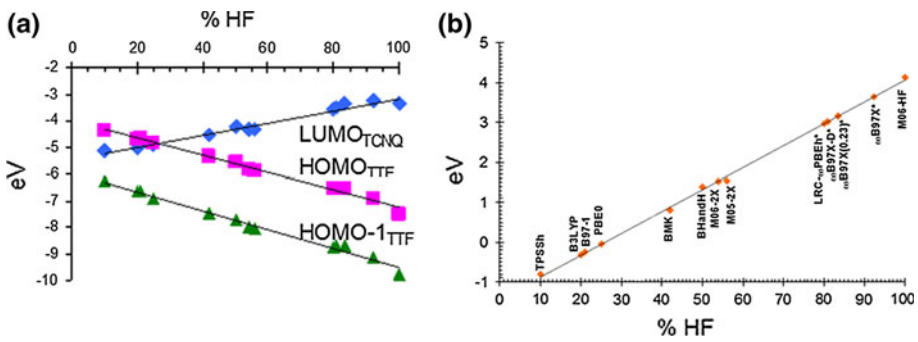

Fig. 1 **a** Computed $HOMO_{TTF}$, $HOMO\text{-}1_{TTF}$, and $LUMO_{TCNQ}$ energies as a function of the percentage of HF exchange. The %HF for ω-functionals are effective values (see text for details). **b** Computed E[$HOMO_{TTF}$]-E[$LUMO_{TCNQ}$] for various DFT functionals varying by the degree of HF exchange (*orange diamonds*). This figure is adapted from [9]

number of electrons). On the other hand, the HF HOMO–LUMO gap is too large compared to the fundamental gap. Thus, the inclusion of some amount of exact exchange by constructing hybrid functionals can improve the comparison between the HOMO–LUMO gap and the fundamental gap. Note that hybrid functionals can be considered as a special case of the generalized Kohn–Sham (GKS) scheme [24–26] designed with the intention to remedy the DFT gap problem. For the TTF/TCNQ example, the M06-HF functional, which contains 100 % HF exchange, provides for the largest E[$LUMO_{TCNQ}$]-E[$HOMO_{TTF}$] energy gap among all DFT functionals considered here, slightly over 4 eV. It is topped only by the HF value itself, 4.87 eV. At the other extreme, the TPSSh functional (that contains just 10 % HF exchange) and the other functionals with a low fraction of HF exchange (B3LYP, B97-1, and PBE0) yield the $LUMO_{TCNQ}$ lower in energy than the $HOMO_{TTF}$. Since the experimental gas-phase values for the ionization potential of TTF and the (exothermic) electron affinity of TCNQ are 6.7 eV [27] and 2.8 eV [28], respectively, this behavior is qualitatively wrong and represents an artifact of these methodologies. Given that a positive value for E[$HOMO_{TTF}$]-E[$LUMO_{TCNQ}$] should be expected, the functionals containing more than 40–50 % HF exchange (i.e., BMK, BHandH, M05-2X, M06-2X, and M06-HF) and the ω-functionals provide at least a reasonably physical description. Comparing the theoretical energy differences with the difference between the experimental IP value for TTF and EA value for TCNQ (3.9 eV), it is found that the ωB97X with a standard value for $\omega = 0.3$ provides reliable results. With regard to the LRC, or ω-functionals, it is not possible to assign explicit values for the percentage of HF exchange. A simple linear regression was used [9] to approximate the relationship between the computed gaps and the percentage of exact exchange, see Fig. 1. This relation has been employed to assign *effective* percentages of exact exchange to the ω-functionals. As we will show, a proper description of the GKS HOMO–LUMO gap will become increasingly important as we build from the example of a single TTF and a single TCNQ to the model interfaces considered below.

2.2 Isolated stacks

A proper description of interfacial electronic properties requires going beyond a simple two-molecule representation containing one donor and one acceptor unit [10]. In order to assess the validity of LRC functionals for systems of large size, we have computed the evolution of the $HOMO_{TTF}$ and $LUMO_{TCNQ}$ in isolated one-dimensional stacks containing from one to five layers. We compared the ωB97X functional, which gave the most reliable results in the previous section, to the BHLYP functional that also

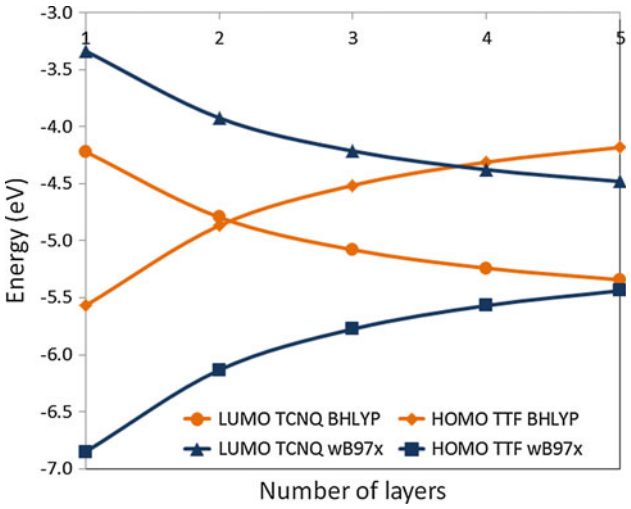

Fig. 2 Evolution of the energy of the HOMO of TTF and LUMO of TCNQ in isolated stacks of growing size, as calculated with the BHLYP and ωB97X functionals. This figure is adapted from [10]

ensures a positive HOMO–LUMO gap for isolated molecules. Figure 2 exhibits a rapid inversion of the two energy levels with BHLYP: $LUMO_{TCNQ}$ lies below $HOMO_{TTF}$ already for a stack of two layers. On the other hand, no inversion is observed with ωB97X and $HOMO_{TTF}$ always stays below $LUMO_{TCNQ}$. Though the shape of the curves is similar for both functionals, it is the initial wider gap of the LRC functional that prevents the levels to cross at least for the stack sizes under consideration. It is worth noticing that such an inversion does occur in the three-dimensional band structure of the TTF/TCNQ co-crystal that presents adjacent columns of TTF and TCNQ molecules (in contrast to the interfacial geometry considered below) due to the increased widths of the bands [29].

2.3 TTF/TCNQ complex

As a first step, we have studied the influence of the nature of the functional on the charge-transfer character in the ground state of a cofacial TTF/TCNQ complex with the two molecules separated by $\sim$3.5 Å. It is worth stressing that CASSCF and CAS-MRCI calculations, used as benchmark in the previous studies, rule out a complete electron transfer in the ground state [9, 10]. Only a partial charge transfer (lower than 0.15 |e|) takes place, which validates the use of a mono-determinantal closed-shell approach such as DFT. However, the shift of the frontier orbitals correlated with the amount of HF exchange should affect the amount of charge transferred.

The electronic coupling between the HOMO of TTF and LUMO of TCNQ generally governs the amount of charge transfer and is very sensitive to the relative orientations/positions of the molecules forming the complex [30]. This is

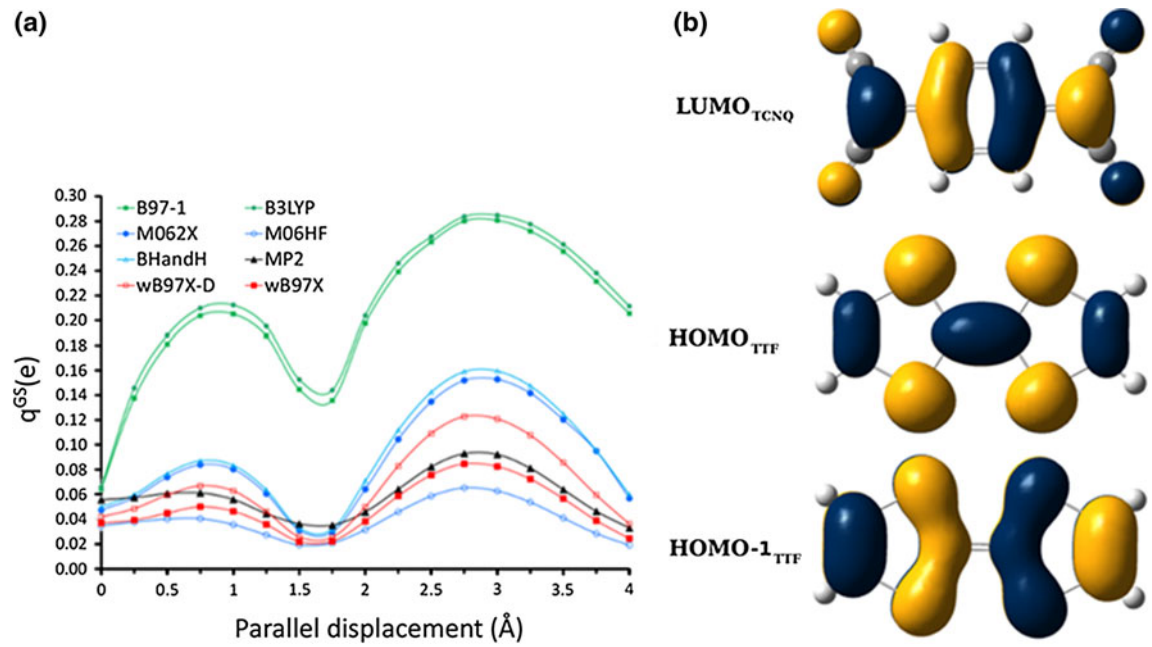

Fig. 3 **a** NPA charges transferred in the ground state (q^{GS}), as calculated with the different functionals, plotted as a function of the horizontal displacement at a fixed interplanar distance of 3.45 Å for the TTF/TCNQ model system. **b** Sketch of the HOMO-1_{TTF}, $HOMO_{TTF}$, and $LUMO_{TCNQ}$ orbitals. This figure is adapted from [9]

shown in Fig. 3a that depicts the evolution of the natural population analysis (NPA) charge q^{GS} transferred as a function of the longitudinal displacement of one molecule of the complex. For a given parallel-displaced geometry, the $HOMO_{TTF}/LUMO_{TCNQ}$ overlap (and the corresponding electronic coupling) varies as a function of the relative positions of the $HOMO_{TTF}$ and $LUMO_{TCNQ}$ nodal surfaces displayed in Fig. 3b. The minimum observed in the q^{GS} values for parallel displacements around 1.75 Å and the maximum observed for displacements of ca. 3.0 Å are consistent with the $HOMO_{TTF}/LUMO_{TCNQ}$ couplings of 0.075 and 0.708 eV calculated at these geometries, respectively, using the procedure described in Ref. [9] (absolute values with the ωB97X functional). The importance of employing functionals with a high admixture of HF exchange can be seen when considering the q^{GS} values for the parallel-displaced structures obtained with B3LYP and B97-1, which greatly overestimate the contribution from the $HOMO_{TTF}/LUMO_{TCNQ}$ coupling and underestimate the energy gap, and as a result, the amount of charge transferred. For a given geometry, the electronic coupling can still vary largely as a function of the choice of DFT functional. This is demonstrated in Fig. 4, where the electronic coupling between HOMO-1_{TTF} and $LUMO_{TCNQ}$ follows a nearly linear dependence upon the amount of exchange, increasing by a factor of $\sim$2.3 in going from the TPSSh functional (10 % HF) to the M06-HF functional (100 % HF).

The natural population analysis (NPA) charges in the ground state (q^{GS}) for the cofacial and the parallel-displaced

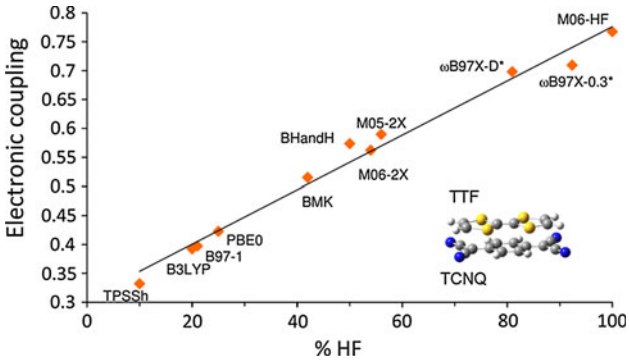

Fig. 4 Electronic coupling (eV) between HOMO-1_{TTF} and $LUMO_{TCNQ}$ for the cofacial TTF/TCNQ model system (with an intermolecular distance of 3.45 Å), as calculated with various functionals and plotted as a function of % HF exchange. This figure is adapted from [9]

configuration at 3.0 Å are plotted in Fig. 5 as a function of the fraction of exact exchange. For the perfectly cofacial geometry, the ground-state charge transfer varies by only 0.05 e^- among the functionals, with a maximum value of 0.08 |e| for TPSSh. The small values calculated in the case of the cofacial geometry are a consequence of the symmetry of the $HOMO_{TTF}$ and $LUMO_{TCNQ}$ orbitals (Fig. 3b), which leads to a vanishing electronic coupling. The small charge transfer in fact arises from interactions between HOMO-1_{TTF} and $LUMO_{TCNQ}$ (which have a larger energy difference). This situation is very different in the

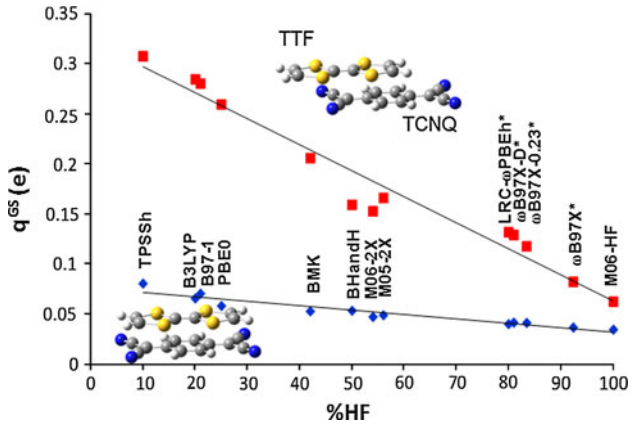

Fig. 5 NPA charge transferred in the ground state (qGS) calculated with the different functionals plotted as a function of the HF exchange for the cofacial (*blue*) and parallel-displaced (*red*) configurations of the TTF/TCNQ model complex. This figure is adapted from [9]

parallel-displaced configuration where the amount of charge transferred increases by up to 0.3 |e|, see Fig. 5.

The poor description of the frontier orbital energies provided by functionals containing only a small percentage of HF exchange (i.e., TPSSh, B97-1, B3LYP, and PBE0) results in an overestimation of the q^{GS} values. On the other hand, the functionals containing more than 50 %HF exchange (i.e., BHandH, M052X, M062X, M06HF, and the ω-functionals) give q^{GS} values lower than 0.2 e^-. When considering the MP2 value of 0.095 e^- as a reference, it can be seen that the ωB97X functional, with the standard value for ω (0.23 $bohr^{-1}$), provides reliable results. This is also consistent with the comparison made above between the computed HOMO–LUMO gaps and the $\sim$3.9 eV experimental difference between IP(TTF) and EA(TCNQ), for which the ωB97X functional also provides a reasonable estimate (namely 3.65 eV).

2.4 Large TTF/TCNQ stacks

We now turn to a description of the evolution of the charge transfer between cofacial TTF and TCNQ stacks of increasing size using different DFT functionals. We start here with the displaced geometry of the complex characterized by a 3-Å translation (that yields the largest charge transfer) and include additional TTF and TCNQ molecules in perfect cofacial orientation. This results in a slip-stacked structure between a cofacial stack of TTF and a cofacial stack of TCNQ. The term "layer" used in the following corresponds to one molecule of TTF and one molecule of TCNQ on each side. For example, the stack represented in Fig. 6a has three layers (i.e., 3 TTF and 3 TCNQ).

The evolution with stack size of the dipole moment along the stacking axis, as calculated with BHLYP and a SVP basis set, is presented in Fig. 6a which clearly shows that the dipole moment along the stacking axis reaches unrealistic values of about 90 Debyes in the largest stacks; in addition, no convergence is reached with system size. This behavior appears to be in contradiction with UPS measurements that point to a vacuum level shift around 0.6 eV, associated with a much smaller interface dipole [31, 32]. In order to understand the origin of these large dipole moments, we have performed a Mulliken charge analysis on a stack comprising six layers, see Fig. 7a.

Figure 7a highlights the large delocalization of the charges within the entire stack. The molecules at the interface bear a significant charge that decreases along the stack though without vanishing at the end of the stack. The evolution with stack size of the charge distribution

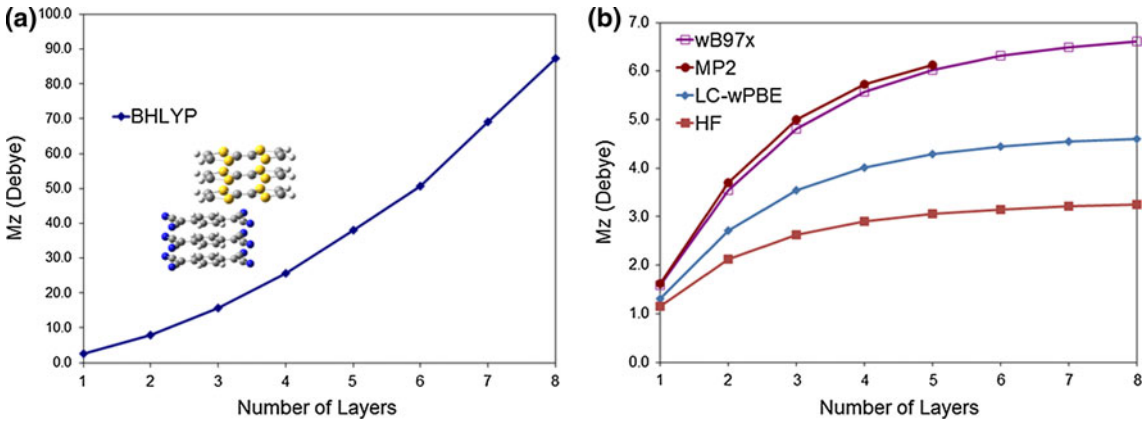

Fig. 6 **a** Evolution of the dipole moment along the stacking axis with an increasing number of layers, as calculated with the BHLYP functional; N layers correspond to a stack including N TTF and N TCNQ molecules. **b** Evolution of the dipole moment along the stacking axis with the number of layers for two long-range-corrected DFT functionals (LC-ωPBE and ωB97X), MP2 and HF methodologies (SVP basis set). This figure is adapted from [10]

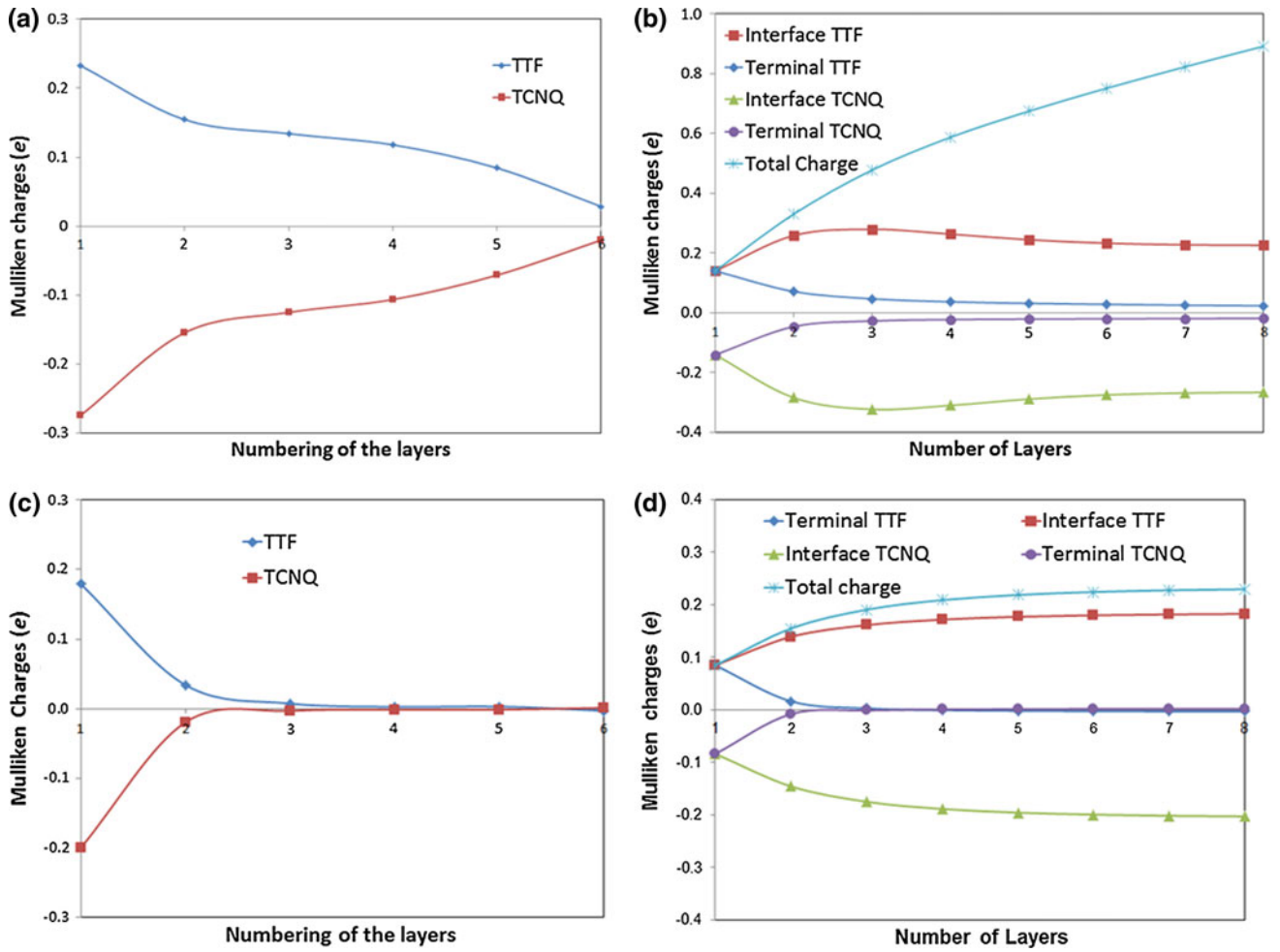

Fig. 7 **a** Evolution of the charge per molecule within a stack of six layers, as calculated with BHLYP (*blue diamond*: charges on TTF—*red square*: charges on TCNQ); layer 1 stands next to the interface. **b** Evolution of the charge (BHLYP) on the interfacial and terminal TTF or TCNQ molecule as a function of stack size, from one to eight layers. **c** Evolution of the charge per molecule within a stack of six layers, as calculated with ωB97X (*blue diamond*: charges on TTF—*red square*: charges on TCNQ); layer 1 stands next to the interface. **d** Evolution of the charge (ωB97X) on the interfacial and the terminal TTF or TCNQ molecule as a function of stack size, from one to eight layers. This figure is adapted from [10]

(BHLYP) in the interfacial and terminal molecules is depicted in Fig. 7b. The charge on the interfacial TTF and TCNQ molecule progressively increases in going from one to three layers and starts slowly decreasing beyond four layers. On the other hand, the charge on the terminal TTF or TCNQ molecule is reduced with the increase in stack size, though a residual charge is always present on the outermost molecule, which explains the continuous increase in dipole moment (Fig. 6a). In addition, the total charge transferred between the two sides of the stack also increases gradually with the size of the system (Fig. 7b). This unphysical evolution of the dipole moment linked with the rapid crossing of $LUMO_{TCNQ}$ and $HOMO_{TTF}$ discussed above rules out the use of BHLYP to study extended donor–acceptor complexes. The pronounced charge delocalization is most likely related to the poor description of the long-range interactions in the BHLYP functional. Accordingly, we next turn to LRC functionals and present in Fig. 6b the evolution of the dipole for stacks containing from one to eight layers, using the LC-ωPBE and ωB97X functionals as well as Hartree–Fock and MP2 methods with the SVP basis set.

The dipole moment calculated with LC-ωPBE and ωB97X for an eight-layer stack amounts to 4.61 and 6.61 D, respectively, and appears to have nearly converged. Furthermore, ωB97X fits best the values obtained with MP2 considered as benchmark. Note that the dipole moment calculated with the HF method converges with the number of layers, but tends to an upper limit around 3.25 D for a stack of eight layers due to the HOMO–LUMO gap overestimation which reduces the amount of charge transfer. In order to understand the difference in behavior

between BHLYP and ωB97X, the Mulliken charge distribution within a stack of six TTF/TCNQ layers obtained at the ωB97X level (Fig. 7c, d) has been compared with the corresponding distribution at the BHLYP level (Fig. 7a, b).

Figure 7 illustrates that the charges are delocalized along the entire stack with the BHLYP functional. On the other hand, the charge distribution obtained with ωB97X is strongly localized on the interfacial molecules. It gets vanishingly small already on the third layer of the stack and decreases even further away from the interfacial region. This evolution explains the saturation of the dipole moment.

Speculating about the performance of the ωB97X functional and, from a broader point of view, about the reasons of success or failure of a given density functional approximation (DFA), the following should be taken into account. There are a number of inherent shortcomings that may affect DFAs, namely the self-interaction error (SIE), the absence of derivative discontinuities (DD), and the wrong description of the asymptotic behavior of Coulomb terms which are all intricately related. In turn, there are well-documented systematic failures of DFAs that are a priori a direct consequence of these limitations. Understanding the relationship between the shortcomings and failures of DFAs is important in order to look for remedies but not always simple, so that a partial remedy often precedes complete understanding. It is therefore difficult to clearly identify which improvement in the ωB97X functional determines its success in our study. Indeed, the main motivation for using LRC hybrid functionals is initially to cure the wrong asymptotic behavior. To do so, the Hartree–Fock exchange is fully (e.g., LC-ωPBE, ωB97X) or partially (e.g., CAM-B3LYP) restored in the long-range (LR) component of the 1/r potential separated for this purpose in two parts with the help of a partition function. The short-range (SR) component remains treated as before range separation is introduced, with a local (e.g., ωB97) or semilocal (e.g., ωB97X) DFA. The reason for which it is preferable to introduce HF exchange in the LR only rather than everywhere in space can be related to a subtle balance of errors between exchange and correlation components of optimized XC DFAs in the electron-rich SR. Interestingly, it was quickly noticed that some LRC functionals are particularly successful in improving on the DD and SIE shortcomings. Altogether, this contributes to a better description of charge transfer between non-covalently bound fragments [33, 34].

2.5 Two-dimensional interfaces

The use of a simple vertical stack is clearly a very crude model to describe the electronic processes taking place at most organic/organic interfaces. It has been previously shown that the depolarization effects in aggregates of higher dimensionality can strongly reduce the interfacial dipole [35–37]. In order to gauge this effect, we have performed 2D periodic boundary conditions (PBC) calculations along the *x*- and *y*-axes (perpendicular to the stacking axis) to replicate the perfect vertical stack considered in the previous section. The PBC method implemented within Gaussian 09 was used with the functionals and basis set that perform best for the individual stack, that is, ωB97X and SVP. The lattice parameters are equal to a = 7.5 Å and b = 11.5 Å, resulting in a distance of 3.1 Å between the closest atoms of a given molecule and its image. The size of the stack considered for the PBC calculations was limited to four layers of TTF/TCNQ molecules since it has been previously observed (Fig. 7c) that the charges per molecule vanish almost completely beyond three layers.

The calculated dipole moments are collected in Table 1 and drop when moving from 1D to 2D structures. This decrease can be as large as 80 % of the initial value in some cases. The saturation of the dipole moment along the z-axis for a stack of three layers correlates well with the Mulliken charge distributions presented in Table 2. These charges are mostly confined within the interfacial layer when applying PBC in the plane while they are more delocalized for an isolated out-of-plane stack.

Table 1 Evolution of the dipole moment (in Debye) along the z-axis as a function of the number of layers using PBC along the (*x*, *y*) plane versus the dipole moment obtained for the isolated stacks

Number of layers	μ_z (D)—PBC	μ_z (D)—isolated stack
1	0.725	1.593
2	0.764	3.547
3	0.982	4.811
4	0.984	5.570

The values are presented for stacks size from one to four layers

Table 2 Mulliken charges on TTF and TCNQ within the first and second layers for the isolated stack and for the stack repeated along the *x*- and *y*- axes using PBC for stacks from one to four layers

Charges |e|	1	2	3	4
Isolated stack				
TTF layer 2	–	0.016	0.027	0.029
TTF interface	0.084	0.139	0.161	0.129
TCNQ interface	−0.084	−0.146	−0.175	−0.148
TCNQ layer 2	–	−0.008	−0.013	−0.015
PBC				
TTF layer 2	–	0.003	0.005	0.004
TTF interface	0.060	0.071	0.070	0.070
TCNQ interface	−0.060	−0.072	−0.074	−0.074
TCNQ layer 2	–	−0.001	0.000	−0.001

3 Conclusions

This work stresses the importance of choosing the appropriate DFT functional to describe the electronic properties at an organic/organic interface. For this purpose, we have investigated, for model donor/acceptor systems, the evolution of the frontier orbital energies with an increased fraction of exact exchange. There, a linear increase in the HOMO–LUMO gap is observed as a function of the percentage of HF exchange, and the ωB97X functional was identified as the most promising functional in comparison with experimental data. The underestimation of the $HOMO_{TTF}/LUMO_{TCNQ}$ gap for functionals with a small amount of HF exchange was found to be the dominating factor explaining the drastic overestimation of the partial charge transferred for a TTF/TCNQ complex placed in a cofacial position. In addition, for large stacks of TTF/TCNQ, the BHLYP functional with 50 % HF exchange shows a disproportionate charge delocalization that results in an unrealistic interface dipole. Again, the ωB97X functional gives a much more realistic behavior in comparison with the values obtained with MP2, which underlines the importance of a well-balanced description of the short- and long-range interactions.

Finally, we have highlighted the major impact of the depolarization effects on the amount of charge transferred at a model interface, using periodic boundary conditions. A drop in interface dipole by as much as 80 % of the value obtained for an isolated stack can be observed.

Acknowledgments The authors acknowledge the European project MINOTOR (FP7-NMP-228424) for financial support. The work in Mons is also partly supported by the Interuniversity Attraction Pole IAP 6/27 of the Belgian Federal Government and by the Belgian National Fund for Scientific Research (FNRS/FRFC). J.C. and D.B. are FNRS Research Fellows. The work at Georgia Tech has been partly supported by the Center for Advanced Molecular Photovoltaics, Award No. KUS-C1-015-21, made by King Abdullah University of Science and Technology (KAUST); the Georgia Research Alliance; and the STC Program of the National Science Foundation under Award DMR-0120967.

References

1. Shen C, Kahn A, Hill I (2001) In: Salaneck WR, Seki K, Kahn A, Pireaux J-J (eds) Conjugated polymer and molecular interfaces: science and technology for photonic and optoelectronic applications. Marcel Dekker, New York, pp 351–400
2. Veenstra SC, Jonkman HT (2003) J Polym Sci Pol Phys 41:2549
3. Ishii H, Sugiyama K, Ito E, Seki K (1999) Adv Mater 11:605
4. Braun S, Salaneck WR, Fahlman M (2009) Adv Mater 21:1450–1472
5. Verlaak S, Beljonne D, Cheyns D, Rolin C, Linares M, Castet F, Cornil J, Heremans Adv P (2009) Funct Mater 19:3809–3815
6. Geskin V, Stadler R, Cornil J (2009) Phys Rev B 80:085411
7. Mulliken RS, Person WB (1969) J Am Chem Soc 91:3409
8. Avilov I, Geskin V, Cornil J (2009) Adv Funct Mater 19:624–633
9. Sini G, Sears JS, Brédas J-L (2011) J Chem Theory Comput 7:602–609
10. Van Regemorter T, Guillaume M, Fuchs A, Lennartz C, Geskin V, Beljonne D, Cornil J, J Chem Phys (submitted to)
11. Becke AD (1993) J Chem Phys 98:5648–5652
12. Lee CT, Yang WT, Parr RG (1988) Phys Rev B 37:785–789
13. Tao JM, Perdew JP, Staroverov VN, Scuseria GE (2003) Phys Rev Lett 91:146401
14. Hamprecht FA, Cohen AJ, Tozer DJ, Handy NC (1998) J Chem Phys 109:6264–6271
15. Ernzerhof M, Scuseria GE (1999) J Chem Phys 110:5029–5036
16. Adamo C, Barone V (1999) J Chem Phys 110:6158–6170
17. Boese AD, Martin JML (2004) J Chem Phys 121:3405–3416
18. as implemeted in Gaussian09
19. Zhao Y, Schultz NE, Truhlar DG (2006) J Chem Theory Comput 2:364–382
20. Zhao Y, Truhlar DG (2008) Acc Chem Res 41:157–167
21. Chai JD, Head-Gordon M (2008) J Chem Phys 128:084106
22. Chai JD, Head-Gordon M (2008) Phys Chem Chem Phys 10:6615–6620
23. Rohrdanz MA, Martins KM, Herbert JM (2009) J Chem Phys 130:054112
24. Seidl A, Görling A, Vogl P, Majewski JA, Levy M (1996) Phys Rev B 53:3764
25. Kronik L, Stein T, Refaely-Abramson S, Baer R (2012) J Chem Theory Comput 8:1515
26. Lichtenberger DL, Johnston RL, Hinkelmann K, Suzuki T, Wudl F (1990) J Am Chem Soc 112:3302–3307
27. Compton RN, Cooper CD (1977) J Chem Phys 66:4325–4329
28. Ishibashi S, Kohyama M (2000) Phys Rev B 62:7839
29. Fraxedas J et al (2003) Phys Rev B 68:195115
30. Brédas JL, Calbert JP, da Silva DA, Cornil J (2002) Proc Natl Acad Sci USA 99:5804–5809
31. Braun S, Liu X, Salaneck WR, Fahlman M (2010) Org Electron 11:212–217
32. Yuge R, Miyazaki A, Enoki T, Tamada K, Nakamura F, Hara M (2002) J Phys Chem B 106:6894–6901
33. Vydrov OA, Scuseria GE, Perdew JP (2007) J Chem Phys 126:154109
34. Haunschild R, Henderson TM, Jiménez-Hoyos CA, Scuseria GE (2010) J Chem Phys 133:134116
35. Cornil D, Olivier Y, Geskin V, Cornil J (2007) Adv Funct Mater 17:1143–1148
36. Natan A, Kronik L, Haick H, Tung RT (2007) Adv Mater 19:4103–4117
37. Heimel G, Rissner F, Zojer E (2010) Adv Mater 22:2494–2513